Study Of the Variation of Thermal Properties of Lead-Free Ceramics of Boron Sodium Gadolinate Niobate at Morphotropic Phase Boundary Following Photo Pyro Electric (PPE) Detection Method

Nissamuddeen Kunnath
Department of Physics, PSMO College (Autonomous) Tirurangadi, Malappuram, 676306, India.

***Abstract*—Nontoxic lead-free ceramics of Boron Sodium Gadolinate Niobate nanocomposites with the general formula (1-x) $BNaGdO_3$ x-$BNaNbO_3$ were synthesized following hydrothermal method followed by solid state sintering with Poly Vinyl Alcohol (PVA) used as the binder. PXRD and SEM analysis revealed that the composite holds a Morphotropic Phase Boundary (MPB) involving the coexistence of rhombohedral and monoclinic phases for the composition with x=0.55. The phase constituents, microstructures and the thermal properties viz., thermal diffusivity, effusivity, specific heat capacity and thermal conductivity are determined and reported. The variation of the thermal properties with the induction of MPB structure was analyzed. This analysis gives much insight into the actual mechanism of phonon vibration mediated heat conduction in solids.**

***Index Terms*—Lead free ceramics, Boron Sodium Gadolinate Niobate (BNGN), PXRD, SEM, Morphotropic Phase Boundary (MPB), Photo Pyro Electric (PPE) detection, thermal diffusivity, effusivity, specific heat capacity, thermal conductivity**

I. INTRODUCTION

Ferroelectric materials produce spontaneous polarizations that are sensitive to many external effects such as electric field, mechanical deformations, temperature and chemical/biological conditions. This has resulted in their use in various sensing applications like gas sensors, chemical sensors, piezoresistive sensors of mechano-thermal signals, photo detectors, ionizing radiation detectors, biosensors, pyroelectric and piezoelectric sensors etc. [1-5]. The development of nanotechnology has revolutionized the field of ferroelectric sensors with development of nanoscale ferroelectrics with excellent properties such as photovoltaic sensitivity, non-linear optical activity, pyroelectricity, direct and inverse piezoelectricity etc. This exceptional combination of different properties enables them to find fascinating applications in Field Effect Transistors,

Non-volatile secondary memories, Capacitors, Photovoltaic cells, Piezoelectric energy harvesters and Micro positioning systems [6-10]. This has resulted in the emergence of ferroelectric nano sensors due to better performance of Nanostructured sensors compared to their bulk counterparts [11-13]. Two prominent class of ferroelectric materials are pyroelectric and piezoelectric materials that produce spontaneous polarization in response to an external change of temperature and pressure (or mechanical stress) respectively. Development of nanostructured pyroelectric and piezoelectric materials has given new possibilities in the field of pyroelectric sensors and piezoelectric transduction materials [14, 15].

Pyroelectric Infra-Red (PIR) detectors are popular due to their room temperature performance and wide spectral response. This performance at ambient temperatures gives them the privileges of low power consumption, broad wavelength response, high stability and sensitivity [16, 17]. Piezoelectric actuators and sensors form micro-electro-mechanical systems with a number of advantages that include instant response, very large output force, low power dissipation, solid body and related convenience for design. The major drawbacks associated with these sensors are hysteresis, creep and vibration sensitivity. However,

among these, creep can be ignored since short lasting durations only are involved and vibration sensitivity can be reduced by damping controls. Hysteresis effects can be reduced to negligible levels by refining the synthesis methods. Hysteresis effect is found to cause around 15% error that rises to around 35% at high frequencies in the case of bulk materials [18, 19].

Crystal asymmetry and spontaneous polarization form the foundation of ferroelectricity, pyroelectricity and piezoelectricity. All ferroelectrics are pyroelectric with their natural electric polarization being reversible. There are 21 non-centrosymmetric classes, among which 20 are piezoelectric, and among this 10 are simultaneously pyroelectric as well. Some of the pyroelectrics that possess natural spontaneous polarization are ferroelectric. Thus, ferroelectrics form a subclass of pyroelectrics which are in fact a subclass of piezoelectric materials.

Recent trends in research on pyroelectric and piezoelectric materials mainly focus on two aspects. The first one is improvement in properties by synthesizing nanostructured materials and composites formed from two chemically different compounds leading to the same property. The second one is the development of non-hazardous environment friendly materials, supporting sustainable development theory; however, in materials with spontaneous polarization able development. During the formation of composites, generally properties follow a mean field and composite formation is associated with several effects, particularly phase change that can lead to polarization catastrophe, resulting in tremendous enhancement of properties that strongly depend on polarization. The latter finding is very important in the current perspective of developing green materials for sustainable development. Correspondingly industries based on such materials have shown very high growth during the last decade.

This work presents and discusses synthesis and characterization of environment friendly, non-hazardous nanoceramic materials of Boron Sodium Gadolinate Niobate (BNGN) from perovskite structured, phase pure Boron Sodium Gadolinate (BNG) and Boron Sodium Niobate (BNN) with potentially high dielectric, pyroelectric and piezoelectric properties. The work involves the trial to enhance the properties by scaling the materials down to nanometer ranges, and introduction of a composition dependent phase change through composite formation. In perovskite materials, for the enhancement of spontaneous polarization and polarization dependent properties, the relative ion sizes of the cubic structures are quite stringent. The ionic radius of Gd^{3+}, Nb^{5+}, B^{3+} and Na^{+} are $0.94A^0$, $0.74\ A^0$, $0.27\ A^0$, $0.99\ A^0$ and their unit cell dimensions a, b, c, d is $1.078\ A^0$, $0.88\ A^0$, $0.41\ A^0$, $1.13\ A^0$ respectively [20, 21]. This indicates that exchange of Gd^{3+} and Nb^{5+} will result in drastic changes in unit cell dimensions and hence the polarizability of the composite material.

None of the elements present in BNGN composites are found to have human toxicity or environmental hazardless. Gadolinium is a ductile rare earth element that show excellent ferromagnetic properties. In its stable form of occurrence in earth in the form of chelated Gadolinium (III) salts, no toxicity has been reported and due to its good paramagnetic properties chelated organo-metallic Gadolinium (III) complexes are used as intravenously administered gadolinium-based MRI contrast agents in medical magnetic resonance imaging [22]. Niobium is a rare, soft, malleable and ductile transition metal with resemblance to Tantalum in its physical and chemical properties. Niobium is generally inert to acids, and even to aqua - regia at room temperature. Niobium is nontoxic with no cases of human poisoning being reported. On exposure to very high concentrations of Niobium nitride or Niobium pentoxide, of the order of $40mg / m^3$, it found to cause scarring of lungs in laboratory animals. Further, no negative environmental effects have been reported for Niobium. In the case of other elements involved in the composites, like Sodium and Boron, also no toxicity or adverse environmental effects have been reported, illustrating that novel BNGN nanocomposites are environment friendly.

The motive of this investigation is to synthesize nanoparticles of BNG and BNN, and then BNGN nanocomposites following a comparatively easy sintering method that could offer controlled texture growth to a large extent and ascertain uniform particle size distribution. We have analyzed the crystal structure variations with composition change, and identified the threshold composition with phase coexistence that offer maximum spontaneous polarization. Their structural, dielectric, thermal, pyroelectric and piezoelectric properties have been investigated and estimated the piezoelectric figures of merits to identify the possibility of using these

composites as green materials for piezoelectric and pyroelectric transducer applications. Hydrothermal synthesis is followed to synthesize phase pure BNG and BNN nanoceramics, and BNGN nanocomposites are synthesized following high temperature sintering. Pelletized BNGN nano powders have been obtained by mixing pure BNG and BNN in desired weight ratios for experimentation.

II. EXPERIMENTAL TECHNIQUES

Procedures followed for the synthesis and processing of pure BNG and BNN nanoceramics and different BNGN composites are described in detail below, followed by various characterization methods and measurements conducted on the samples.

2.1 Synthesis of Nano powders of pure BNG and BNN

Nano powders of Boron Sodium Gadolinate (BNG) and Boron Sodium Niobate (BNN) were synthesized following conventional hydrothermal route. The reagents used for the synthesis were Boric anhydride (B_2O_3, Sigma Aldrich, 99.9% pure) as Boron precursor, Sodium hydroxide (NaOH) to provide the alkaline reaction media, Gadolinium oxide (Gd_2O_3, Aldrich, 99.9% pure) and Niobium oxide (Nb_2O_5, Aldrich, 99.9% pure) as the precursors for Gadolinium and Niobium respectively. A highly alkaline medium (9M-12M) was always preferred for hydrothermal synthesis since it offered uniform particle size distribution and mature formation of the nanoparticles [23]. For the synthesis of BNG a powder mixture of Gadolinium oxide and Boric anhydride, maintaining a 2:1 ratio between B and Gd, was charged to a 12M solution of NaOH in double distilled water under magnetic stirring and stirred vigorously for 3 hours to obtain a pale-yellow solution. The reaction mixture was then transferred to a Teflon lined autoclave and treated hydrothermally for 5 days at 175^0C and at an ambient pressure of 1.5 bars. BNN nano powders were also synthesized following an identical procedure. A ratio 2:1 of Boron to Niobium was maintained in the reaction mixture and hydrothermal treatment was carried out under the same conditions used for BNG. A high initial pH of the order of 10 - 12 for the reaction mixture has a crucial role in the formation of perovskite nanostructures, as a low initial pH generally resulted in the formation of metal oxide nanoparticles instead of complex perovskite nanoparticles [24].

After the reaction time the autoclave was naturally cooled inside the furnace and the precipitated nanoparticles were collected by centrifugation and washed several times by dispersing in double distilled water and dried overnight at an ambient temperature of 75^0C. The nano powders of BNN and BNG obtained in this way were then calcined at 600^0C to remove any volatile impurities present.

2.2 Preparation of BNGN Nanocomposites with MPB

The fine perovskite nano powders of BNN and BNG in desired weight ratios were mixed, ground and pelletized using Poly Vinyl Alcohol (PVA) used as the binder to obtain ceramic ceramic nanocomposites with the general formula (1-x) $BNaGdO_3$ – x-$BNaNbO_3$. In order to induce Morphotropic phase boundary, x was varied from 0 to 1, taking values 0.0, 0.20, 0.25, 0.33, 0.55, 0.66, 0.75, 0.80 and 1.0, where samples with x=0.0 and 1.0 correspond to pure BNG and BNN respectively. Thin ceramic pellets of BNGN nanoparticles having 9 mm diameter and thickness below 0.5mm were prepared and then calcined at 600 ^{0}C. The samples were then subjected to solid state sintering at 1000 ^{0}C for a duration of 12 hours.

2.3 Characterization of the samples

Powder XRD analysis of all the composites were conducted using a Bruker D8 Advance X-ray diffractometer, using Copper K-α radiation of wavelength 1.5406 A^0. Powder XRD enables one to confirm the nano nature of the composites and to identify the crystalline phases in them. The angle 2Θ was varied from 3^0 to 70^0 at a step size of 0.1^0 with time per step being 100 seconds. The crystallite sizes of the composites were determined using the Debye Scherer formula. Crystal density was evaluated from XRD using standard formulae and a comparison of this density with experimental values were carried out to analyze the porosity of the samples. The lattice constants (a, b, c) and the unit cell volume (V) were evaluated from the XRD data using the MAUD program and the results of the calculations were used to identify valuable information about the variation of the phase with composition and the occurrence of MPB, if any.

The microstructure and surface morphology of the composites were recorded using a Scanning electron microscope (JEOL 6390 LV).

2.4 Sample Density Measurements

As ceramic – ceramic composites have been processed

following solid-state sintering, there are strong chances for the occurrence of pores in the sample. These will be reflected as extraordinary deviations of the experimental density from corresponding theoretical values. A crucial consequence of porosity of ceramics is that it causes deviations from expected properties, particularly dielectric and piezoelectric properties [25]. We have measured the densities of all the samples following Archimedes method, and compared them with corresponding theoretical densities, obtained from crystallographic data drawn from XRD. The relative porosity of various composites is also investigated by evaluating the percentage porosity using the relation,

$$\% \text{ porosity} = \frac{(Theoretical\ Density - Experimental\ Density)}{Theoretical\ Density} \times 100 \quad (1)$$

An extreme low porosity, as small as possible, is always required for further treatments like electric poling and the measurements of thermal, dielectric, pyroelectric and piezoelectric properties.

2.5 Measurement of Thermal Properties

Thermal properties of BNGN ceramics, thermal diffusivity, thermal effusivity, thermal conductivity and specific heat capacity, have been determined following a photothermal technique, with a pyroelectric detector used as the thermal detector [30]. In this method intense light from a laser source is intensity modulated using a mechanical chopper and made to impinge on the surface of the sample under measurement. When the sample has high reflectivity, an extremely thin coating of fine carbon black may be provided on the surface of the sample. The sample absorbs a part of the incident energy and undergoes a non-radiative de - excitation, resulting in a periodic heating of the sample. This causes periodic temperature variations in the sample which could be directly detected using the sensitive pyroelectric transducer to which the sample is attached using a heat sinking, electrically resistant Greece. The application of heat sinking Greece to attach the pyroelectric detector to the sample has two advantages: the compound supports heat transfer from the sample to the detector fluently, and it suppresses the transfer of any pyroelectrically or piezoelectrically induced voltage to the detector and the backing medium, reducing possibility for any experimental errors. A 120 mW He-Cd laser with wavelength 442nm was used as the heating light source. A Nickel- Chromium alloy coated PVDF film was used as the pyroelectric detector. Due to the high electrical resistance, but high thermal conductivity of Nickel-Chromium alloys the thermal waves propagating from the sample will be coupled to the detector, whereas the unwanted noise emf originating from vibration and thermal agitation will be omitted. These make the PPE experimental set up a versatile one, particularly for piezoelectric and pyroelectric materials used in this work.

The sample-detector assembly was mounted on a thermally thick backing. The modulation frequency of light was kept above 60 Hz to ensure that the detector, the sample and the backing were thermally thick during measurements. The output signals as amplitude and phase were recorded with a dual-phase lock-in amplifier (Make: Stanford Research Systems, Model: SR830). Measurement of amplitude and phase of the output signal enabled us to determine the thermal diffusivity (α) and thermal effusivity (e), from which the thermal conductivity (k) and specific heat capacity (C) of the samples could be obtained.

III. RESULTS

Results of investigations, regarding the change in crystal structure induced by change of composition leading to MPB, and the outcome of measurement of various properties are presented and discussed in this session. Generally, in the case of composite materials the dielectric, pyroelectric, piezoelectric and thermal properties follow a mean field approximation or the so called effective medium theory. It is possible to predict and calculate the properties of various composites using the relevant equations following effective medium theory which is somewhat similar to determination of mass number of elements with isotopes as the weighted average of mass of various isotopes in terms of their relative abundance. For instance, the equations to evaluate the specific heat capacity, according to effective medium theory, is given below [31, 32].

$$C_{eff} = \phi_f C_f + (1- \phi_f) C_m \text{ ----------(2)}$$

where ϕ and C represent the volume fraction and specific heat capacity and the subscripts, m, f, eff respectively represent the relevant parameters of the matrix, filler and composite respectively. The assumptions and approximations of the effective medium theory are well documented in the cited references.

In spite of the above predictions of the effective medium theory, the results on BNGN nanocomposites do not follow these with regard to their properties and there are some other effects that influence their properties. These are also presented and discussed in this session.

3.1 Bulk density of samples and porosity

As these ceramic-ceramic composites are processed following solid-state sintering, there is strong chance for the occurrence of pores in the sample which will be immediately reflected as extraordinary deviation of the experimental density from the theoretical values. A very crucial consequence of porosity of the ceramics is that it causes severe changes to their properties, particularly the dielectric and piezoelectric properties [33]. So, it is inevitable that density measurements are conducted and a good agreement between theoretical density, evaluated using effective medium theory, and experimental density, obtained from Archimedes method are in good agreement.

Figure 1 shows the variations of theoretical and experimental densities of various BNGN compositions. The theoretical densities of the composites are determined using the rule of mixtures as,

$$\rho_{eff} = \phi_f \rho_f + (1- \phi_f) \rho_m \text{----------(3)}$$

where ρ is the density. The densities of phase pure BNG and BNN, evaluated from XRD data, are found to be 3.352 g/cc and 4.003g/cc respectively. Using these values of density, the mass densities of the composites are determined using Equation (3). The densities of various BNGN ceramics are also determined following Archimedes method, which is reported as the experimental density. As can be seen in Figure 1 the theoretical and experimental densities are in good agreement.

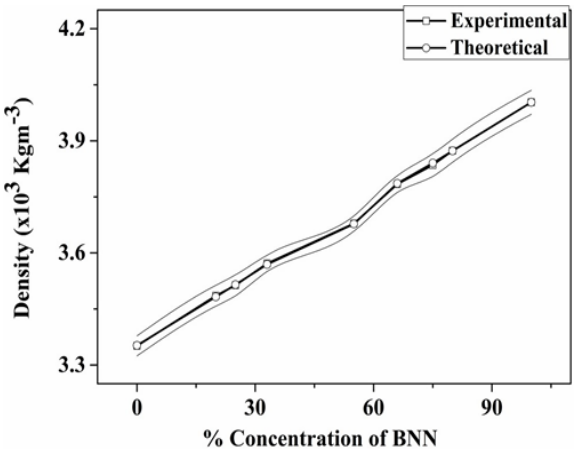

Fig. 1: Variations of mass density (theoretical and experimental) with concentration of BNN in BNGN ceramics

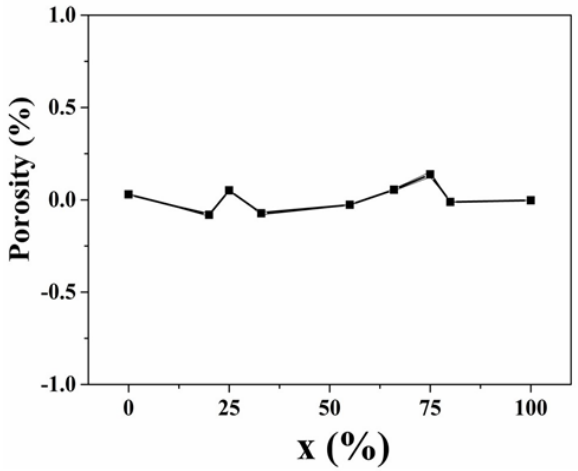

Fig. 2: Variation of porosity with concentration of BNN in BNGN ceramics

The porosity of BNGN nanocomposites, evaluated from the corresponding densities, are found to be less than 1%, as is evident from Figure 2. Thus, we infer that the composites have achieved density as per their original requirement and the porosities in the samples are very small to cause any change of properties.

3.2 Structure and Morphology

Figure 3 shows the Powder XRD spectrum of (1-x) $B_{0.5}Na_{0.5}GdO_3$ - x- $B_{0.5}Na_{0.5}NbO_3$ composites with increasing concentration of BNN composition (labelled in the inset as x), so that x=0 and 1 respectively represent the spectra of pure BNG and BNN. The JCPDS matching of pure BNG and BNN have been performed and the labelling of peaks in terms of Miller indices have been

done. The crystallite size of the composites is evaluated from the XRD peaks using Debye Scherrer formula and are found to be around 68.21nm, 48.65nm, 61.76 nm, 37.02 nm, 28.94nm, 47.58nm, 55.52nm, 49.98nm and 64.87nm
respectively for the compositions with x=0, 0.20, 0.25, 0.33, 0.55, 0.66, 0.75, 0.80 and 1.00. This confirms that the composites formed are nano ceramics, and further it can be noticed that the crystallite sizes of all the composites, on an average, are less than that of pure BNN and BNG ceramics. This indicates that BNN and BNG with perovskite structure and general formulae $B_{0.5}Na_{0.5}NbO_3$ and $B_{0.5}Na_{0.5}GdO_3$ respectively are diffused in to each other to form composite perovskite structures with general formula (1-x) $B_{0.5}Na_{0.5}GdO_3$ - x- $B_{0.5}Na_{0.5}NbO_3$.

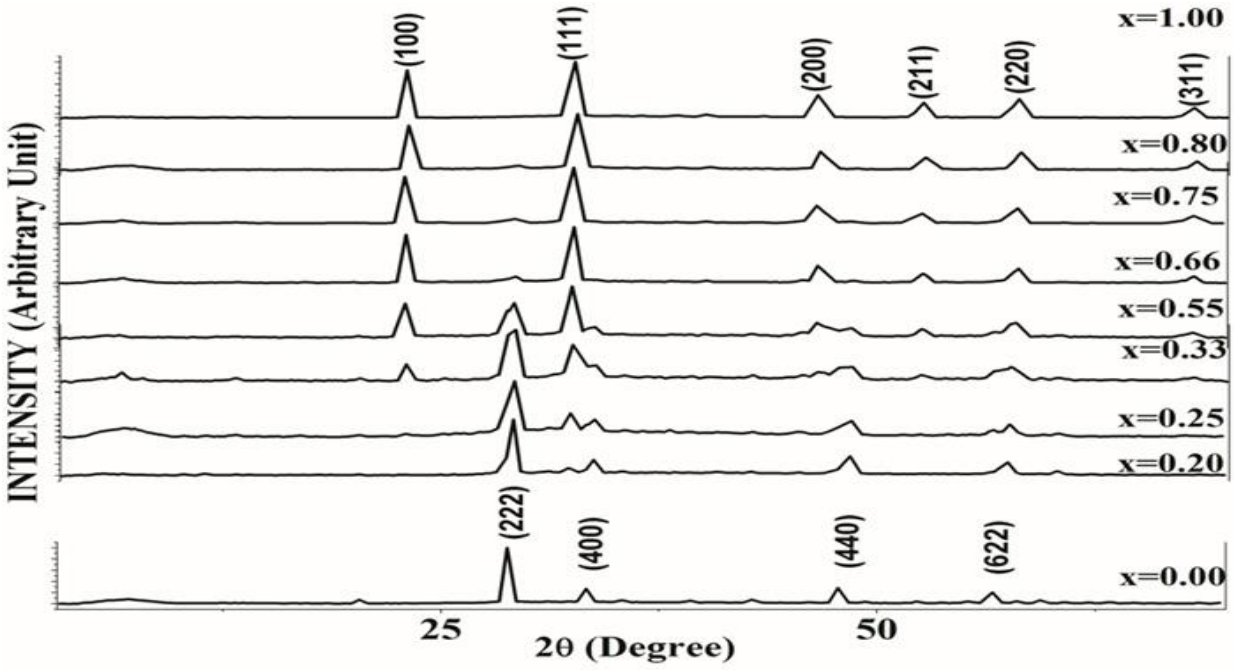

Fig. 3: Powder XRD patterns of hydrothermally synthesized BNGN (1-x) $B_{0.5}Na_{0.5}GdO_3$- x $B_{0.5}Na_{0.5}NbO_3$ with x=0 (pure BNG), 0.20, 0.25, 0.33, 0.55, 0.66, 0.75, 0.80 and 1.00 (pure BNN), all sintered at 1000^0C for 12 hours.

All BNGN compositions exhibit perovskite structure with no secondary phase formation being observed. Pure BNG nanoceramics (JCPDS 431014) crystallizes in rhombohedral structure with lattice constants a= 10.742 A^0, b=10.742 A^0 and c=10.751 A^0 as obtained from analysis using MAUD program. Whereas pure nanoceramics of BNN is identified to have a monoclinic structure with 2m space group (JCPDS 331207) and the lattice parameters from MAUD program are found to be a=8.563 A^0 b=10.754 A^0 and c=13.561 A^0. The XRD analysis reveals that the BNGN composites show a transition from rhombohedral to monoclinic lattice structure with increasing concentration of BNN. The rhombohedral structure of BNGN composites is characterized by a single sharp (222) peak at $2\Theta = 28.804^0$ and another (440) peak at $2\Theta = 47.751^0$, whereas the Monoclinic structure is characterized by (111) and (400) peak splitting between 2Θ of 32.52^0 and 33.34^0 and a (200) and (440) peak splitting between 2Θ values of 46.42^0 and 47.75^0. The former one begins to sharpen and the latter one is considerable in the case of composition with x=0.55. It can also be seen from the figure that the (222) peak and the (400) peak shift towards the higher angle range as the concentration of BNN is increased. The peak splitting of
(111) / (400) peak and (200) / (440) peak indicate the coexistence of rhombohedral and monoclinic phases in the composites implying the existence of a morphotropic phase boundary in these composites [34].
Results supporting the above analysis of XRD measurements are obtained from microstructural analysis by SEM. Figure 4 shows the SEM

micrographs of phase pure BNG (Fig. 4(a)), BNN (Fig.4(i)) and BNGN composites with x = 0.20, 0.25, 0.33, 0.55, 0.66, 0.75, 0.80 respectively from Fig. 4(b) to Fig. 4(h), all sintered at 1000^0C for 12 hours. Figures in the inset represent the images with ten times higher resolution. From the images 4(a) and 4(i) it can be seen that pure BNG particles possess nearly hexagonal morphology where as that of BNN is almost cubic. Further, BNG and BNN particles show only single phases whereas two distinct phases of varying extent of growth can readily be seen in all composite BNGN particles. These are being further shown in the enlarged insets in Fig. 4(a) to 4(i) and are further confirmed from EDS analysis. EDS analysis reveal that the light grey phase is perovskite $B_{0.5}Na_{0.5}NbO_3$ whereas the pale silver white phase corresponds to $B_{0.5}Na_{0.5}GdO_3$ perovskite structure. The miscibility of the two major phases can distinctly be seen from composition with x=0.25 (Fig. 4(c)) onwards. From this composition onwards it can also be seen that a massive needle like structure starts growing that become vivid in composition with x=0.33 (Fig. 4(d)). The needle structure become the prominent phase in Fig. 4 (e) and 4(f) where they have diameters of the order of a few hundreds of nanometers and length extending up to a few micrometers. The needle structure persists to the composition with x=0.8 (Fig 4(h)) and even in pure BNN, though not absolutely vivid. This further confirms that the compositions involve the coexistence of rhombohedral and monoclinic phases in varying extents and this coexistence is at its maximum for the composition with x=0.55, indicating the existence of a morphotropic phase boundary at this composition [35].

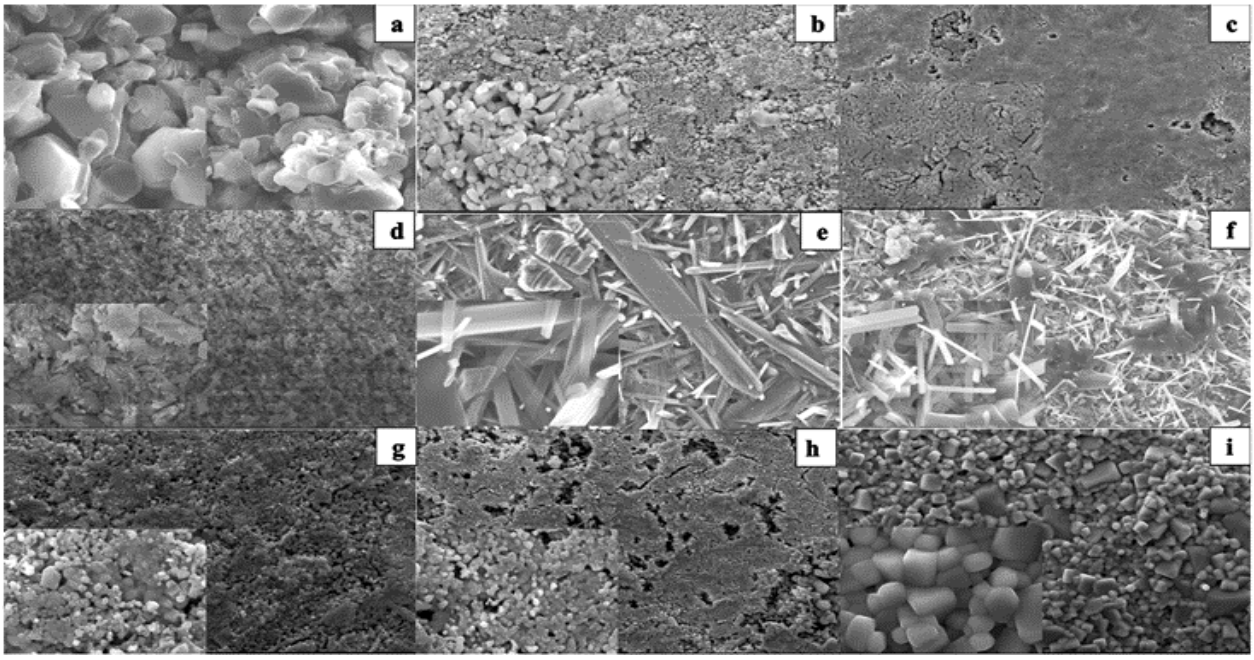

Fig. 4. SEM images of hydrothermally synthesized BNGN nanoceramics $(1-x)\ B_{0.5}Na_{0.5}GdO_3$- $x\ B_{0.5}Na_{0.5}NbO_3$ with x=0 (pure BNG), 0.20, 0.25, 0.33, 0.50, 0.66, 0.75, 0.80 and 1.00 (pure BNN), all sintered at 1000^0C for a duration of 12 hours. Images with ten times higher resolution are shown in the inset.

3.3 Thermal Properties

The thermal diffusivity, thermal effusivity, specific heat capacity and thermal conductivity of all the BNGN composites were determined using the indigenously built photo pyroelectric experimental set up. The PPE amplitude and phase of the samples enable a direct determination of thermal diffusivity and thermal effusivity. The variation of PPE amplitude and phase of various BNGN nanocomposites were recorded using a dual phase lock-in amplifier as a function of modulating frequency. The variations of PPE amplitude and phase of pure BNG, BNN and some of the representative BNGN composites are shown in Figures 5 and 6 respectively. Similar variations have

been obtained for PPE amplitude and phase for other BNGN composites.

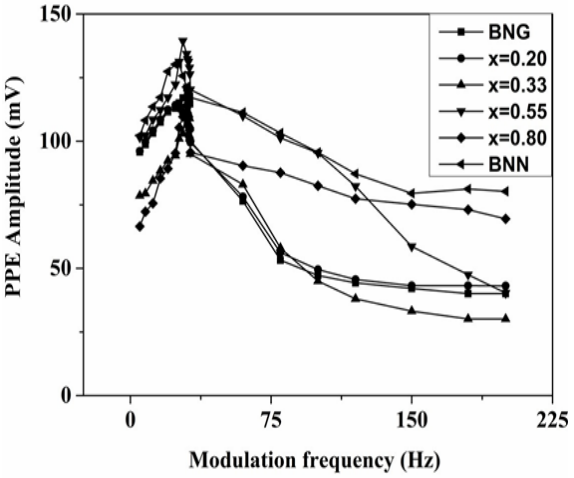

Fig. 5: Frequency dependence of photopyroelectric amplitudes with modulation frequency at room temperature for the Samples shown in the inset.

While conducting measurement of thermal parameters of solids that have piezoelectric and /or pyroelectric properties following photopyroelectric method, there is a chance for enhancement of the PPE amplitude signal due to piezoelectric or pyroelectric or both the effects [37]. This problem arises from the piezoelectric properties of the pyroelectric detector as well, which causes an additional signal arising from the pressure that the samples insert on the pyroelectric detector. Since the all the BNGN composites are found to be strongly pyroelectric and the PVDF detector is found to have considerable piezoelectric response there is a chance for large noise generation upon the pyroelectric voltage signal due to piezoelectric contribution of the detector and pyroelectric contribution of the samples. Under such a circumstance the linear relationship between frequency and PPE amplitude and phase in the thermally thick region of the samples will be lost. In the experimental set up this problem is overcome by using a nickel chromium alloy coated PVDF film as the detector which offer high electrical resistance at the surface of the detector to which the sample is attached. The sample is attached to the detector using a non–electrically conducting coating of a heat sinking grease. This coupling fluid layer of Silicone grease guarantee thermal coupling between the sample and detector, at the same time prevent any voltage developed at the sample due to pyroelectric properties of the sample to reach the detector. Further, the fluid nature of grease makes the mechanical coupling small enough to prevent the thermal strain induced in the sample by the thermal wave being transmitted to the detector and hence a purely pyroelectric voltage is recorded. However, when the grease freezes at low temperature it become very stiff and transmit the thermal strain to the detector causing noise generation. All the measurements in this work are performed at room temperature only. It may be mentioned that at temperature lower than about 230K, grease solidifies and accurate determination of thermal parameters require further modification for the experimental setup.

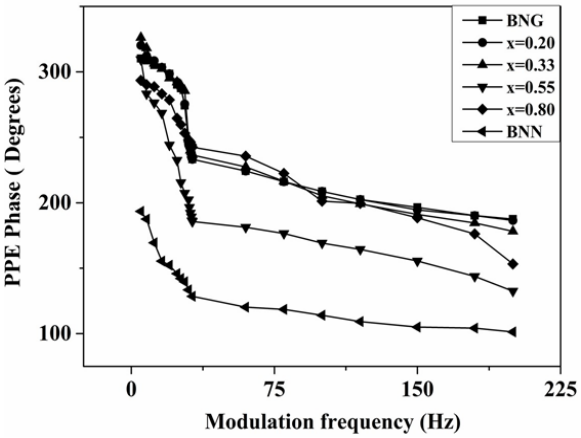

Fig. 6: Frequency dependence of photopyroelectric phases with modulation frequency at room temperature for the Samples shown in the inset.

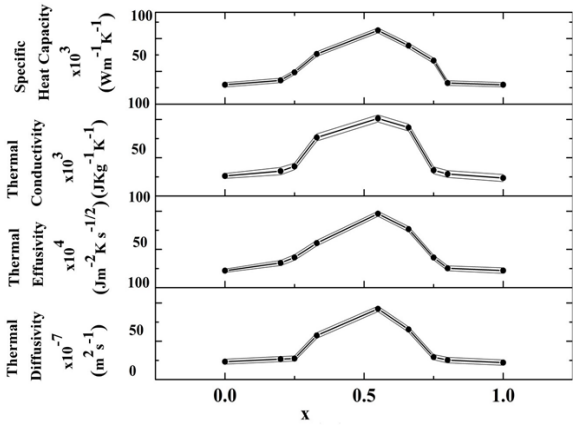

Fig. 7: Variations of thermal diffusivity, thermal effusivity, thermal conductivity and specific heat capacity for BNGN samples with fractional composition of BNN (x)

The thermal diffusivity, thermal effusivity, thermal conductivity and specific heat capacity of all the

samples have been determined from the PPE amplitude and phase [34]. The variations of all these with percentage composition of BNN are shown in Figure 7. It can be noted that thermal diffusivity and effusivity shows a steep raise from x = 0.33 to x=0.55, the MPB composition and fall thereafter. The thermal conductivity and specific heat capacity also follow a similar trend though the values do not show a steep variation closer to MPB, instead the composition closer to MPB on both sides also have values of conductivity and specific heat capacity comparable to that of the MPB composition. It can also be noticed from Figure 5.15 that phase pure BNG and BNN have thermal properties that are comparable and composites with very low composition of either BNG or BNN have values of thermal properties that more or less follow a mean field approximation. However, the thermal properties show a quite extraordinary behavior once the composition is closer to MPB.

IV. DISCUSSION OF RESULTS

It is seen that in BNGN ceramics the theoretical densities, evaluated following the mean field approximation, and experimental densities, determined following Archimedes method, are in good agreement. This indicate that the ceramics are non-porous and the porosity has no effect on the control of mechanical, dielectric, pyroelectric or piezoelectric properties. There are a number of factors that affect the porosity of a ceramic material. This includes presence of pore forming agents, mechanical properties, miscibility of constituents, sintering temperatures, ceramic additives, metallic additives and coatings etc. In the case of BNGN composites the constituents are highly miscible and the only factor that has a determining role in the porosity of samples is the sintering temperature. Since sintering was carried out at 1000^0C for a considerably longer duration, no porosity is expected in the composites. This is further confirmed by evaluating the percentage porosity using the relation (1). The percentage porosity of all the composites is less than 1%, as is evident from Figure 2.

In order to confirm the existence of rhombohedral to monoclinic MPB in BNGN composites, as evident from PXRD analysis, the lattice parameters of all the composites are evaluated using MAUD program and indices corresponding to monoclinic and rhombohedral structures have been evaluated. The values of lattice parameters of the compositions are tabulated in Table 1, along with the variation of lattice parameters with BNN content in the composites. This variation of lattice parameters with percentage concentration of BNN is plotted in Figure 8. As is evident from the Table and the Figure the lattice constants for compositions with x up to 0.2 correspond to rhombohedral structure whereas the lattice starts to deviate from rhombohedral structure for compositions with x > 0.33.

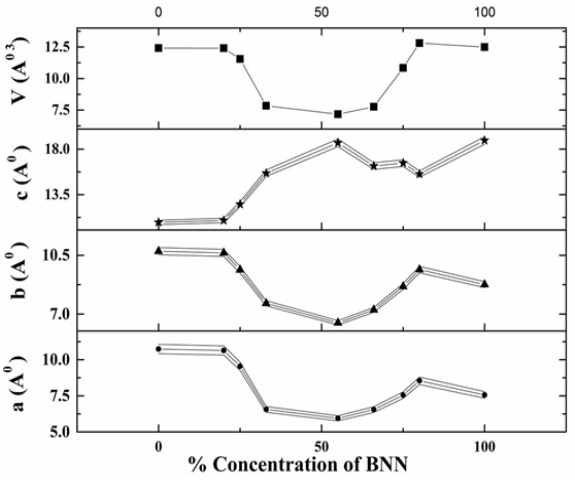

Fig. 8: Variation of lattice parameters with percentage concentration of BNN

The lattice parameters have a trend to retain monoclinic structure for all compositions above x=0.33, including phase pure BNN. However, the monoclinic structure parameter c/a is found to be maximum in the case of composition with x=0.55 where the rhombohedral structure factor b/a is 1.091, which deviates from 1 drastically for all compositions below and above this. This further confirms the coexistence of rhombohedral and monoclinic phases in the composition with x=0.55 and hence account for the MPB structure. It is also noticed that the unit cell volume falls considerably towards the MPB structure with the composition holding MPB structure having minimum unit cell volume. It is anticipated that the occurrence of monoclinic and rhombohedral phases together in this composition make it susceptible to large orientation polarization resulting in the enhancement of polarization dependent electrical properties, suggesting it as promising material for transducer applications [35].

For compositions with x up to 0.25 the rhombohedral

strain constant shows perfect matching and is evidently equal to 1. However, as the composition parameter x exceed 0.25 there occures a gradual deviation from rhombohedral geometry as the rhombohedral strain constant (b/a) increases above 1, indicating the development of lattice parameters b and c different from a. A corresponding increase in the monoclinic strain parameters c/b and c/a are also evident, which correspond to the deviation from rhombohedral geometry, with the monoclinic strain factor found to peak to a threshold high value at composition with x = 0.55, where c appears to have an increase of 300% compared to the composition with x = 0 or pure BNN. In the case of compositions with x < 0.55 the strain constants b/a, c/a and c/b are more or less equal to 1, indicating a rhombohedral phase with slight deviation corresponding to an increase in concentration of BNN. This deviation is maximum in the case of composition with x = 0.55, where the phase is predominantly monoclinic with a standard monoclinic unit cell. For concentration above x = 0.55, the monoclinic phase is retained, but the unit cell changes from standard monoclinic unit cell to tilted oblique rhombic prism unit cell of the monoclinic phase. Thus, clearly the composition with x = 0.55 correspond to the phase of coexistence of rhombohedral and monoclinic phases.

Table 1: Lattice parameters of BNGN composites for different concentrations of BNN

X	Lattice Parameters						
(%)	a (A^0)	b (A^0)	c (A^0)	V ($A^{0\,3}$)	b/a	c/b	c/a
0	10.742±0.008	10.742±0.007	10.751±0.005	1240.56	1.000	1.001	1.001
20	10.642±0.005	10.642±0.005	10.947±0.024	1239.75	1.000	1.029	1.029
25	9.549±0.004	9.632±0.024	12.552±0.014	1154.48	1.009	1.303	1.314
33	6.565±0.022	7.643±0.021	15.623±0.022	783.904	1.164	2.044	2.38
55	5.942±0.006	6.483±0.022	18.628±0.017	717.588	1.091	2.873	3.135
66	6.549±0.011	7.253±0.022	16.331±0.022	775.721	1.108	2.252	2.494
75	7.549±0.006	8.642±0.025	16.622±0.012	1084.39	1.145	1.923	2.202
80	8.543±0.024	9.642±0.016	15.541±0.007	1280.14	1.129	1.612	1.819
100	7.563±0.022	8.754±0.011	18.862±0.012	1248.79	1.158	2.155	2.494

The phase coexistence has a number of consequences and resultant impacts on the spontaneous polarization and thermal properties of the crystal. In pure rhombohedral phase there are eight ferroelectric domains and there are five ferroelectric domains in pure monoclinic phase [38, 39]. In the case of composition with MPB, however, there occur a sharp increase in the number of polarizable ferroelectric domains from a maximum of eight or five to 13, with a large number of these 13 ferroelectric domains being easily polarizable. It is found that in monoclinic phase the polarization vector has rotational symmetry [40, 41] in a symmetry plane, allowing it to have unrestricted rotation of polarization vector in an applied external electric field. This rotation of polarization vector in monoclinic phase is theoretically predicted by Fu, Cohen and Bellaiche [42 - 45] and is experimentally confirmed by B Noheda et al [46]. This freedom of rotation of monoclinic phase can largely contribute to the spontaneous polarization of the crystal.

The thermal properties such as thermal diffusivity, effusivity, specific heat capacity and thermal conductivity depend mainly on lattice vibrations in the solid. More precisely, lattice vibrations (phonons) are responsible for the characteristic properties of solids such as thermal properties, electrical conductivity, optical and dielectric properties, diffusion mechanism, phase changes etc. In the case of nanostructures, the interaction of phonons and hence thermal properties are critically controlled by dimensional confinement of phonon modes, similar to confinement of electrons in a quantum well. The dimensional confinement of phonons results in restrictions in phase space for phonon wave vectors, due to which carrier-phonon interactions in nanostructures are modified by phonon confinement.

The specific heat capacity of a solid is given by,

$$C_v = \frac{\partial E}{\partial T} \text{----------(4)}$$

where E is the average internal energy of the solid. Both lattice vibrations and thermal motion of electrons contribute to specific heat capacity, with the electronic specific heat being negligible at room temperature. Under such an assumption the equipartition theorem predicts the specific heat capacity of a solid to be constant, given by the Dulong-Petit law as,

$$C_v = 3NK_B \text{----------(5)}$$

However, at low temperatures the specific heat capacity decreases with temperature. Thermal conductivity is a measure of the ease of flow of heat in a solid. In metals heat conduction is via electrons whereas it is entirely via phonons in insulators. The thermal conductivity is given by,

$$K = \frac{1}{3} C_V f l \text{ ----------(6)}$$

Where, C_V is the specific heat, f is the phonon velocity and l are the men free path, with f and l being average quantities over all occupied modes and Brillouin zones.

While analyzing thermal properties of BNGN composites, we notice that these increase with concentration of BNN and found to be maximum for the composition with MPB (x = 0.55), after which it falls. It is also confirmed that the monoclinic distortion is maximum in the case of composition with MPB where the crystal itself is assumed to be under internal distortion. It has been observed that lattice distortion results in a decrease in phonon-phonon and phonon-defect collision rates, resulting in an increase in phonon mean free path [47]. Evidently in view of equation (5.14) the thermal conductivity of the BNGN composites then increases with crystal distortion, whereas at the same time an increase of specific heat capacity with distortion is due to larger contribution of phonon modes due to their softening [48]. The thermal diffusivity (D) and effusivity (e) are related to the conductivity through the following equations [49],

$$D = \frac{K}{\rho C} \text{ ----------(7)}$$

and,

$$e = \sqrt{KC\rho} \text{ ----------(8)}$$

where ρ is the crystal density and c are the specific heat capacity. In view of the above two equations, it is clear that an increase in K results in a proportionate increase in diffusivity and effectivity.

V. CONCLUSIONS

We arrive at the following conclusions from the work presented in this paper:

1) Novel, environment-friendly perovskite nanoceramics of Boron Sodium Gadolinate ($B_{0.5}Na_{0.5}GdO_3$) and Boron Sodium Niobate ($B_{0.5}Na_{0.5}NbO_3$) are successfully synthesized following a comparatively cost-effective method.
2) A morphotropic phase boundary is induced by synthesizing solid solutions of BNGN nanoceramics, with general formula (1-x) B0.5Na0.5GdO3 – xB0.5Na0.5NbO3, for a value of x = 0.55.
3) The phase constituents, microstructures, dielectric and piezoelectric properties of the composites are determined and reported.
4) For the composition with MPB, there occur the coexistence of rhombohedral and monoclinic phases. This MPB is characterized by an extraordinary rise in the c/a lattice parameter ratio of the crystal and a needle like structure formation.
5) The thermal properties of all the BNGN nanocomposites are reported and discussed.

REFERENCES

[1] Zhu, W., et al. "Preparation, Property, and Mechanism Studies of Amorphous Ferroelectric (Ba, Sr) TiO 3 Thin Films for Novel Metal–ferroelectric–metal Type Hydrogen Gas Sensors." Journal of Materials Research 15.6 (2000): 1291-1302.

[2] Wang, L., et al. "Ferroelectric WO3 nanoparticles for acetone selective detection." Chemistry of Materials 20.15 (2008): 4794-4796.

[3] Tan, O. K., et al. "Hydrogen-sensitive I–V characteristics of metal ferroelectric gas sensor device fabricated by sol gel technique." Materials Science and Engineering: B 58.3 (1999): 221-228.

[4] Mistewicz, Krystian. "Recent Advances in

Ferroelectric Nano sensors: Toward Sensitive Detection of Gas, Mechanothermal Signals, and Radiation." Journal of Nanomaterials 2018 (2018).

[5] Park, Jonghwa, et al. "Fingertip skin–inspired microstructured ferroelectric skins discriminate static/dynamic pressure and temperature stimuli." Science advances 1.9 (2015): e1500661.

[6] Nonnenmann, Stephen S., et al. "The ferroelectric field effect within an integrated core/shell nanowire." Advanced Functional Materials 22.23 (2012): 4957-4961

[7] Liu, Xingqiang, et al. "Ferroelectric memory based on nanostructures." Nanoscale research letters 7.1 (2012): 285.

[8] Lu, Haidong, et al. "Nanodomain engineering in ferroelectric capacitors with graphene electrodes." Nano letters 16.10 (2016): 6460-6466.

[9] Jung, Jong Hoon, et al. "Lead-free KNbO3 ferroelectric nanorod based flexible nanogenerators and capacitors." Nanotechnology 23.37 (2012): 375401.

[10] Fei, Linfeng, et al. "Electrospun bismuth ferrite nanofibers for potential applications in ferroelectric photovoltaic devices." ACS applied materials & interfaces 7.6 (2015): 3665-3670.

[11] Liang, Longyue, et al. "One-dimensional ferroelectric nanostructures: synthesis, properties, and applications." Advanced Science 3.7 (2016): 1500358.

[12] Varghese, Justin, Roger W. Whatmore, and Justin D. Holmes. "Ferroelectric nanoparticles, wires and tubes: synthesis, characterisation and applications." Journal of Materials Chemistry C 1.15 (2013): 2618-2638.

[13] Alpay, S. P., V. Nagarajan, and G. A. Rossetti. "Recent developments in ferroelectric nanostructures and multilayers." Journal of Materials Science 44.19 (2009): 5021-5024.

[14] Mistewicz, Krystian. "Recent Advances in Ferroelectric Nanosensors: Toward Sensitive Detection of Gas, Mechanothermal Signals, and Radiation." Journal of Nanomaterials 2018 (2018).

[15] Chi, Ziqiang, and Qingsong Xu. "Recent advances in the control of piezoelectric actuators." International Journal of Advanced Robotic Systems 11.11 (2014): 182.

[16] Spain, E., and A. Venkatanarayanan. "13.02 Review of Physical Principles of Sensing and Types of Sensing Materials." (2012).

[17] Hashmi, Saleem. Comprehensive materials processing. Newnes, 2014.

[18] Ge, Ping, and Musa Jouaneh. "Tracking control of a piezoceramic actuator." IEEE Transactions on control systems technology 4.3 (1996): 209-216.

[19] Li, Qing Xiang, Dong Sheng Wang, and Yu He Li. "Design of modern precision instruments." (2004).

[20] Ahrens, Louis H. "The use of ionization potentials Part 1. Ionic radii of the elements." Geochimica et cosmochimica Acta 2.3 (1952): 155-169.

[21] Pauling, Linus. The Nature of the Chemical Bond... Vol. 260. Ithaca, NY: Cornell university press, 1960.

[22] Ganjali, Mohammad Reza, et al. Lanthanide's series determination by various analytical methods. Elsevier, 2016.

[23] Liao, Wei-Qiang, et al. "A molecular perovskite solid solution with piezoelectricity stronger than lead zirconate titanate." Science 363.6432 (2019): 1206-1210.

[24] Morita, Takeshi. "Piezoelectric materials synthesized by the hydrothermal method and their applications." Materials 3.12 (2010): 5236-5245.

[25] Morita, Takeshi. "Piezoelectric materials synthesized by the hydrothermal method and their applications." Materials 3.12 (2010): 5236-5245.

[26] Whatmore, R. W. "Pyroelectric devices and materials." Reports on progress in physics 49.12 (1986): 1335.

[27] Corsi, Carlo. "Infrared: a key technology for security systems." Advances in Optical technologies 2012 (2012).

[28] Cilulko, Justyna, et al. "Infrared thermal imaging in studies of wild animals." European Journal of Wildlife Research 59.1 (2013): 17-23.

[29] Kad, R. S. "IR thermography is a Condition Monitor Technique in industry." International Journal of Advanced Research in Electrical,

Electronics and Instrumentation Engineering 2.3 (2013): 988-993.

[30] Menon, C. Preethy, and J. Philip. "Simultaneous determination of thermal conductivity and heat capacity near solid state phase transitions by a photopyroelectric technique." Measurement Science and Technology 11.12 (2000): 1744.

[31] Rizvi, Imbesat Hassan, et al. "Mathematical modelling of thermal conductivity for nanofluid considering interfacial nano-layer." Heat and mass transfer 49.4 (2013): 595-600.

[32] Hossain, M. E., et al. "Modelling of high-k dielectric nanocomposites." Acta mechanica 225.4-5 (2014): 1197-1209.

[33] Fuentes, J., et al. "Dielectric and piezoelectric properties of the KNN ceramic compound doped with Li, La and Ta." Applied Physics A 118.2 (2015): 709-715.

[34] Kunnath, Nissamuddeen, and Jacob Philip. "Dielectric and piezoelectric performance of lead-free ceramics of boron sodium gadolinate niobate at morphotropic phase boundary." Journal of Advanced Dielectrics 10.04 (2020): 2050014.

[35] Kalyani, Ajay & Brajesh, Kumar & Senyshyn, Anatoliy & Ranjan, Rajeev. Orthorhombic-tetragonal phase coexistence and enhanced piezo-response at room temperature in Zr, Sn, and Hf modified $BaTiO_3$. Applied Physics Letters 2014. 104: 252906-252906- 5. 10.1063/1.4885516.

[36] Li, Yue-Ming, et al. "Enhancement of piezoelectric properties and temperature stability by forming an MPB in KNN-based lead-free ceramics." Journal of Materials Science: Materials in Electronics 25.2 (2014): 1028-1032.

[37] Salazar, A., and A. Oleaga. "On the piezoelectric contribution to the photopyroelectric signal." Review of scientific instruments 76.3 (2005): 034901.

[38] Bokov, A. A., and Z-G. Ye. "Ferroelectric properties of monoclinic Pb ($Mg_{1/3}$ $Nb_{2/3}$) O_3-$PbTiO_3$ crystals." Physical Review B 66.9 (2002): 094112.

[39] Deng, Hao, et al. "Direct observation of monoclinic ferroelectric phase and domain switching process in ($K_{0.25}$ $Na_{0.75}$) NbO_3 single crystals." CrystEngComm 17.14 (2015): 2872-2877.

[40] Noheda, B., et al. "A monoclinic ferroelectric phase in the Pb (Zr_{1-x} Ti_x) O_3 solid solution." Applied physics letters 74.14 (1999): 2059-2061.

[41] Noheda, Beatriz, et al. "Tetragonal-to-monoclinic phase transition in a ferroelectric perovskite: The structure of $PbZr_{0.52}$ $Ti_{0.48}$ O_3." Physical Review B 61.13 (2000): 8687.

[42] Fu, Huaxiang, and Ronald E. Cohen. "Polarization rotation mechanism for ultrahigh electromechanical response in single- crystal piezoelectrics." Nature 403.6767 (2000): 281-283.

[43] Bellaiche, L., Alberto García, and David Vanderbilt. "Finite- temperature properties of Pb (Zr_{1-x} Ti_x) O_3 alloys from first principles." Physical Review Letters 84.23 (2000): 5427.

[44] Bellaiche, L., Alberto García, and David Vanderbilt. "Electric-field induced polarization paths in P b ($Z r_{1-x}$ Ti_x) O_3 alloys." Physical Review B 64.6 (2001): 060103.

[45] Vanderbilt, David, and Morrel H. Cohen. "Monoclinic and triclinic phases in higher-order Devonshire theory." Physical Review B 63.9 (2001): 094108.

[46] Guo, R., et al. "Origin of the high piezoelectric response in $PbZr_{1-x}$ Ti_x O_3." Physical Review Letters 84.23 (2000): 5423.

[47] Cohn, J. L., et al. "Local lattice distortions and thermal transport in perovskite manganites." Physical Review B 56.14 (1997): R8495.

[48] Krumhansl, J. A., and R. J. Gooding. "Structural phase transitions with little phonon softening and first-order character." Physical Review B 39.5 (1989): 3047.

[49] El-Brolossy, T. A., and S. S. Ibrahim. "Photoacoustic measurement of thermal properties of polystyrene metal oxide composites." Thermochimica acta 509.1-2 (2010): 46-49.

[50] Tang, Yanxue, and Haosu Luo. "Investigation of the electrical properties of (1− x) Pb (Mg1/3Nb2/3) O3–xPbTiO3 single crystals with special reference to pyroelectric detection." Journal of Physics D: Applied Physics 42.7 (2009): 075406.

[51] Yan, Yongke, and Shashank Priya. "High performance textured piezoelectric ceramics and method for manufacturing same." U.S. Patent Application No. 14/351,803.

[52] Kittel, Charles, and John Wiley. Elementary solid-state physics: a short course. Wiley, 1962.

[53] Liu, Wenfeng, and Xiaobing Ren. "Large piezoelectric effect in Pb-free ceramics." Physical review letters 103.25 (2009): 257602